Proceedings of the 2001 IEEE
International Conference on Robotics & Automation
Seoul, Korea • May 21-26, 2001

Nonlinear Control Methods for Planar Carangiform Robot Fish Locomotion

Kristi A. Morgansen[†‡], Vincent Duindam[‡], Richard J. Mason[‡],
Joel W. Burdick[‡], Richard M. Murray[†‡] *

[†]Control and Dynamical Systems [‡]Mechanical Engineering
California Institute of Technology, Mail Code 107-81, Pasadena, CA, 91125
{kristi,vincent,murray}@cds.caltech.edu, {jwb,mason}@robotics.caltech.edu

Abstract: *This paper considers the design of motion control algorithms for robot fish. We present modeling, control design, and experimental trajectory tracking results for an experimental planar robotic fish system that is propelled using carangiform-like locomotion. Our model for the fish's propulsion is based on quasi-steady fluid flow. Using this model, we propose gaits for forward and turning trajectories and analyze system response under such control strategies. Our models and predictions are verified by experiment.*

1 Introduction

This paper investigates the control of fish-like robots that propel themselves by changes in their shape rather than by the use of propellers and maneuvering surfaces. The study of underwater locomotion has long been a subject of interest to the biological community [3, 6, 13]. In the past several years, the robotics and engineering communities have been inspired by this research to construct mechanisms that mimic the behavior of swimming lifeforms. The motivation for this work comes from the high maneuverability that fish demonstrate over conventional propeller-driven underwater vehicles.

Some of the most impressive swimmers in nature propel themselves by the *carangiform* style of swimming. In carangiform swimming, the front two-thirds of the fish's body moves in a largely rigid way, with the propulsive body movements being confined to the rear third of the fish's body—primarily the tail. Carangiform movement is one of the easiest to replicate from a mechanical design perspective. Previous work in this area has come from the robopike and robotuna projects at MIT and Draper Laboratories [1, 2, 15].

Prior robotic fish research has focused on the issue of propulsion efficiency and fluid flow effects and has been primarily empirical. For example, the approach taken in the MIT and Draper Laboratories projects focused on a parameterized kinematic model of the mechanical fish rather than detailed models of the robot fluid-body interaction. The parameters in the model were determined by extensive experimental trials so as to minimize overall system drag. The end result of this effort produced a reproduction of a tuna that swims untethered in open water. However, the accuracy and robustness with which these vehicles can track a trajectory is unknown. Others have recently studied the vortices shed by a pitching and heaving plate [5].

Our work differs from these studies in one main respect: we focus on the issue of motion planning and control. A suitable model for the fluid-body interaction is clearly a prerequisite for control system analysis and design. In previous years, Caltech work in this area has focused on studying the fluid-body interaction using two approaches. The first approach involves a reduced Lagrangian formulation where a fish is taken to be a rigid body with the action of the tail represented by a point vortex of independently controlled position and strength [4]. The second approach is based on a highly simplified quasi-static lift and drag model of the forces on the fish body and tail [8, 9]. Previous papers presented the development of a robotic testbed for planar carangiform locomotion [8]. An updated version of this testbed is used in this paper to verify our approach. Prior papers also presented comparisons between the behavior of the experimental system and the restriction of the model to the case of forward propulsion [9]. Some simple turning maneuvers were also discussed.

In this paper we use methods from nonlinear control theory to generate system inputs which allow our fish-like robot to track simple trajectories. The model for this work is based on a modest extension of the simple quasi-static lift and drag approach previously

*This work was supported in part by the National Science Foundation through an Engineering Research Center grant and through NSF grant CMS-9502224.

proposed. While this model does not capture every detail of the fluid-body interaction, it does serve several useful purposes. First, it allows us to write a description of our system in a control affine form where the control inputs enter linearly. We can therefore apply known methods to analyze control performance. Importantly, we note that the linearized equations are not controllable, precluding the use of standard linear methods for trajectory tracking. However, as we will show, application of recent results in nonlinear control theory demonstrate that we can generate a variety of gaits and achieve trajectory tracking for this system. In particular, our approach predicts "wriggling" sequences that cause turning. These maneuvers would be difficult to find by intuition or by direct adoption of the maneuvers of real fish whose mechanical structure is sufficiently different than our robot fish. Second, it is not absolutely necessary to capture all fluid flow details for the purposes of control design, since control feedback can compensate for reasonable modeling errors. In fact, an important conclusion of our work is that the detailed computational or experimental models of fluid flow that have been developed in prior work [16] are not completely necessary for the purposes of robot fish control system design.

2 Experimental Apparatus

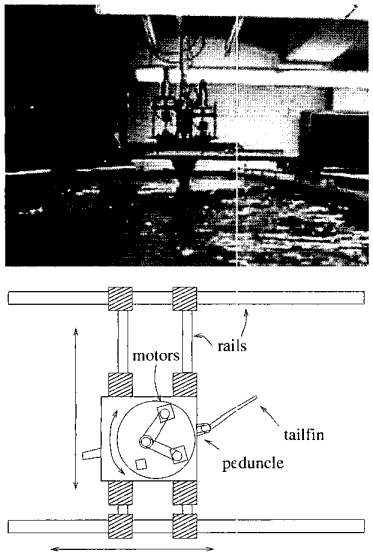

Figure 1: Photograph from rear and schematic of top view of fish design.

To motivate the fluid-body model that is developed in Section 3, we first review our prototype carangiform robot fish testbed. Our robot is a simple approximation to a carangiform-type fish consisting of three links: a flat rectangular "body", a flat rectangular "tail", and an open brace "peduncle" connecting the two (see Figs. 1 and 2). The three-link mechanism is suspended from a passive trolley in a water tank 4 ft wide by 4 ft deep by 36 ft long. The trolley consists of two orthogonal sets of rails and a rotating platform, all supported on low friction bearings. The robot is attached to a shaft that runs through the center of the rotational platform. Thus the robot is free to move in a plane, but the point of body rotation will be determined by the location of the shaft connection to the robot rather than by the robot's center of mass. During tail flapping, the trolley mechanism allows the fish to propel itself and its supporting carriage around the tank. Our assumption of planar motion is not unrealistic and is a typical assumption for the study of fish locomotion [13, 16].

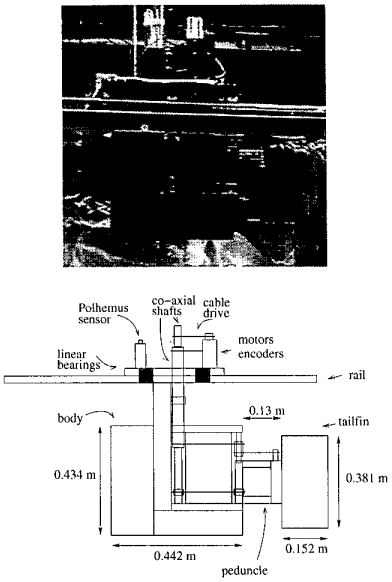

Figure 2: Photograph and schematic of side view of fish design.

The tail and peduncle joints are independently controlled by transmitting torques from two DC motors through a steel cable-drive system. Joint angles are continuously measured via optical shaft encoders mounted on each motor. Position and orientation of the body are measured with a Polhemus sensor attached to the carriage. This sensor is based on magnetic field measurements and has been calibrated to compensate for field distortion effects due to the presence of steel in the lab.

The fish "body" and "tail" consist of a combina-

tion of flat plexiglas plates with dimensions as shown in Fig. 2. The peduncle is an open rigid brace which connects the body to the tail, and we assume it has little hydrodynamic effect. The mass of the entire robot and trolley system is 30 kg, and the inertia of the body with the tail fully extended is $0.5038\ \mathrm{kg}\cdot\mathrm{m}^2$. Because of the tail's small mass relative to the body, we assume that variations in the moment of inertia due to tail motion are negligible. By rotating the peduncle and tail joints, the tail moves back and forth, and its velocity relative to the fluid induces lift, drag, and virtual fluid mass reaction forces which are transmitted to the body via the peduncle.

The nonlinear control methods in which we are interested require that we either begin with a passively stable system or apply closed-loop control to stabilize the system. For our application, the term "passively stable" implies that when the fish is placed in a constant velocity flow, the body and tail will tend to align with the flow–i.e., a "weather-vane" effect. We state without proof that a sufficient condition for passive stability of our system is that the trolley shaft be attached to the body no more than half the body length from the body's front end. Essentially this condition ensures that the drag experienced by the portion of the body behind the shaft is larger than the drag on the front portion of the body. This force imbalance produces moments which cause the body to align with, and pointing into, the flow. Our current design was modified from the original [9] to be stable in this way.

3 A Control Affine Model

This section develops a simplified model for the robot described in Section 2. As discussed in [9], our three-link mechanism is a reasonably general planar approximation to carangiform locomotion, and therefore small modifications of this model should have general utility in the analysis of carangiform swimming.

As we will show, the joint velocities will enter our system equations quadratically. In order to produce a control-affine model where controls enter linearly, we must then take our control inputs to be the angular accelerations of the joints. The result will be a system with ten-dimensional state space and two-dimensional control space. We neglect three-dimensional fluid effects and assume that we can restrict our attention to a plane parallel to the floor. We assume that the forces applied to the system come from quasi-static lift effects, drag effects, and added fluid mass effects on the tail and body.

Fig. 3 shows a simple diagram of the robot with the principal acting forces. Without loss of generality, we assume that the point at which the body is attached

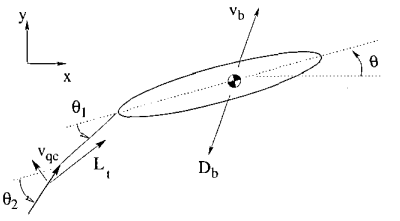

Figure 3: Diagram for control-affine model.

to the trolley shaft coincides with the body center of mass. The body position is given relative to an inertial frame by $[x, y]$ where the positive direction is taken to the right. The body orientation, measured relative to an inertial x-axis, is denoted by θ. When measured relative to the body longitudinal axis, the peduncle and tail angles are denoted by $[\theta_1, \theta_2]$, whereas these angles are denoted by ψ_1 and ψ_2 when they are measured relative to the inertial x-axis. The body has length l_b, the distance between the center of rotation and the peduncle joint is l_{cort}, the peduncle has length l_p, the tail has length l_t, the depth of the body in the water is h_b and the depth of the tail is h_t. The unit vector along the tail plate, $l_{e,t}$ is given by

$$l_{e,t} = [-\cos(\psi_2), -\sin(\psi_2), 0]\,.$$

The angle between the body translational velocity at the center of rotation, $[\dot{x}, \dot{y}, 0]$, and the inertial x-axis is $\alpha_0 = \tan^{-1}(\dot{y}/\dot{x})$.

From standard quasi-steady airfoil theory we know that the lift on a flat plate is given by

$$L = \pi\rho A\,(v_{\mathrm{qc}} \times l_e) \times v_{\mathrm{qc}},$$

and the moment about the quarter chord point by

$$\tau = -\pi\rho\frac{l_f^2}{4}\left(\dot{x}_m\dot{y}_m\cos(2\psi_2) + \frac{1}{2}\left(\dot{y}_m^2 - \dot{x}_m^2\right)\sin(2\psi_2)\right)$$

where A is the surface area of the plate, ρ is the density of the fluid, v_{qc} is the velocity of the plate relative to the flow at a point that is one-quarter of the chord length from the plate's leading edge, and $\dot{x}_m$ and $\dot{y}_m$ are the velocity of the tail at its midpoint. We assume here that the tail does not stall and that the angle of attack never exceeds ninety degrees (which would result in the leading edge becoming the trailing edge). The velocity at the quarter chord point of the tail is

$$v_{qc,t} = \begin{bmatrix} \dot{x} + l_{cort}s_\theta\dot{\theta} - l_p s_{\psi_1}\dot{\psi}_1 - (l_t/4)s_{\psi_2}\dot{\psi}_2 \\ \dot{y} - l_{cort}c_\theta\dot{\theta} + l_p c_{\psi_1}\dot{\psi}_1 + (l_t/4)c_{\psi_2}\dot{\psi}_2 \\ 0 \end{bmatrix}$$

where $s_{(\cdot)} = \sin(\cdot)$ and $c_{(\cdot)} = \cos(\cdot)$.

The drag on a pitching and heaving flat plate is approximated as the projection of the blunt body drag onto the velocity direction. Because the incremental velocity element corresponding to angular rotation depends on position, we must integrate the incremental drag over the plate. For a plate of length l rotating about a point at a distance a from one end of the plate, the drag integration can be evaluated as

$$D = \frac{1}{2}\rho C_D h \int_{a-l}^{a} \|V_a \times r - s\dot{\theta}\| V ds$$

where C_D is the drag coefficient, V_a is the translational velocity at a, r is a unit vector aligned with the plate and $V = V_a + \dot{\theta} r$. Similarly, the moment of the drag force about the point of rotation is given by

$$M_D = \frac{1}{2}\rho C_D h \int_{a-l}^{a} \|V_a \times r - s\dot{\theta}\|(V_a \times r - s\dot{\theta}) s ds.$$

Additionally, we must account for the added mass effect that results from accelerating a rigid body through a fluid. For a flat plate, the effect of moving through water adds a mass of quantity $m_w = 1/4\pi l^2 h$ along the lateral direction of the body-fixed mass matrix where l is the length of the plate and h is its depth.

Collecting these terms results in the equations

$$\begin{bmatrix} \ddot{\psi}_1 \\ \ddot{\psi}_2 \\ m_x \ddot{x} \\ m_y \ddot{y} \\ I_\theta \ddot{\theta} \end{bmatrix} = \begin{bmatrix} u_1 \\ u_2 \\ L_{t,x} + D_{b,x} \\ L_{t,y} + D_{b,y} \\ [x_t, y_t] \times [L_{t,x}, L_{t,y}] + M_{D,b} + \tau \end{bmatrix} \quad (1)$$

where $L_{t,x}$ describes the x-component of the lift force on the body, $D_{b,y}$ describes the tail drag in the y directions, etc. Drag on the tail and lift on the body are small compared to body drag and tail lift and have not been included in this model. To simplify notation, we will sometimes utilize generalized coordinates $[q, \dot{q}]$ where $q = [\psi_1, \psi_2, x, y, \theta]$.

4 Nonlinear Control Background

4.1 Controllability and Accessibility

Given a system of the form $\dot{x} = f(x, u)$, the first question we should ask is whether the system has a controllable linearization either at a point or about a trajectory. While our system does not possess linear controllability at a point, we believe that linearization about a trajectory can be achieved but have not yet been able to verify this result. We must then resort to the use of nonlinear methods. The general form of a two input nonlinear system in control affine form, where controls enter linearly, is

$$\frac{d}{dt}\begin{bmatrix} q \\ \dot{q} \end{bmatrix} = f(q, \dot{q}) + g_1(q, \dot{q})u_1 + g_2(q, \dot{q})u_2. \quad (2)$$

The vector $f(\cdot)$ is referred to as the system drift, and $g_1(\cdot)$ and $g_2(\cdot)$ are termed the control vector fields. The Lie bracket of two vector fields h_i and h_j is denoted $[h_i, h_j] = ad_{h_i} h_j$ and is defined to be $[h_i, h_j] = \frac{\partial h_j}{\partial x} h_i - \frac{\partial h_i}{\partial x} h_j$. Given a set $\mathcal{H}$ of C^∞ vector fields on a manifold M, the Lie algebra of $\mathcal{H}$, $L(\mathcal{H})$ is the set of all Lie brackets of elements of $\mathcal{H}$ and of all the Lie brackets of vector fields generated by Lie bracketing. The family $\mathcal{H}$ satisfies the *Lie algebra rank condition* (LARC) at a point $p \in M$ if the Lie algebra of $\mathcal{H}$ evaluated at p, $L(\mathcal{H})(p)$, is the whole tangent space of M at p. The set $\mathcal{H}$ is said to satisfy the *accessibility property* from a point p if, for every $T > 0$, the set of points reachable from p in time $\leq T$ is nonempty. The following is a standard result [14]:

Proposition 1 *Let $\mathcal{H}$ be a family of C^∞ vector fields on a C^∞ manifold M. Then the* LARC *at p implies accessibility from p.*

A control system $\dot{x} = f(x) + \sum_{i=1}^{m} g_i(x)u_i$ is *small time locally controllable* (STLC) at p if the vector fields $\{f, g_1, \ldots, g_m\}$ satisfy the accessibility property at p and p is contained in the set of points reachable from p in time T for every $T > 0$. This definition requires that a nonlinear system with nonzero drift term satisfies the STLC condition for points p such that $f(p) = 0$. For mechanical systems described with generalized coordinates $[q, \dot{q}]$ these points are simply those for which $\dot{q} = 0$.

4.2 Second-Order Linearly Uncontrollable Systems

Based on the structure of the Lie algebra of our system, we will use some recent results from the control of second-order linearly uncontrollable systems [10, 11] to motivate a choice of control functions. As a starting point, we consider the class of driftless nonholonomic systems which can be written as

$$\dot{x} = \sum_{i=1}^{m} g_i(x)u_i, \quad x \in \mathbb{R}^n \quad (3)$$

and which satisfy m constraints of the form

$$\omega_i(x)\dot{x} = 0, \quad 1 \leq i \leq m.$$

These driftless nonholonomic systems can be extended to two more or less general classes of second-order systems by cascading either the inputs or outputs through a set of integrators. In particular, when

the inputs are passed through a set of integrators, the resulting systems will take the form

$$\dot{\xi} = u, \quad \dot{x} = \sum_{i=1}^{m} g_i(x)\xi_i, \quad \xi \in \mathbb{R}^m. \tag{4}$$

If the underlying nonholonomic system (3) is controllable, then as shown in [10], the cascaded system satisfies the accessibility property with the vector fields shown in the following proposition:

Proposition 2 *Consider a system of the form (4) where the underlying nonholonomic system (3) is controllable with the set of vector fields*

$$\mathcal{G} = \left\{ g_i, ad_{g_{i_1}} g_{i_2}, \ldots, ad_{g_{i_1}} \cdots ad_{g_{i_r}} g_{i_{r+1}} \right\}.$$

Then the system (4) is accessible with the set of vector fields $\{g_i, \tilde{\mathcal{G}}\}$, all brackets in $\mathcal{G}$ are zero and

$$\begin{aligned} \tilde{\mathcal{G}} \;=\; & \left\{ ad_f g_i, ad_{ad_f g_{i_1}} ad_f g_{i_2}, \right. \\ & \left. \ldots, ad_{ad_f g_{i_1}} \cdots ad_{ad_f g_{i_r}} ad_f g_{i_{r+1}} \right\}. \end{aligned}$$

The structure of the Lie brackets of a system determines which control function combinations will generate motions along the different basis directions of the state space. The control vector fields specify which states are linearly influenced by given control functions, and $ad_f g_i$ corresponds to the effect of the system's inertial response after control u_i is applied. The bracket of two control vector fields corresponds to infinitesimal periodic switching between the corresponding controls. Recursive application of these rules determines the combinations of controls that generate motion in different directions of the state space. Practically speaking, with this analysis we can determine which "wrigglings" of the fish joints will generate motion in a given direction.

The notion of generating motion along the direction of Lie bracket vector fields using periodic control functions has led to a variety of nonlinear control methods based on the use of amplitude-modulated time varying sinusoidal control functions with integrally related frequencies. We list the general relations here and refer the reader to [7, 10, 12] for details and examples. As mentioned above, the state space directions corresponding to the control vector fields are directly controlled with the system inputs. Motions corresponding to brackets of two vector fields are generated by a switching between the appropriate controls which can be accomplished using sinusoids ninety degrees out of phase. Second level bracket directions can be produced by cosines of one frequency along two of the control directions and a cosine of twice that frequency along the third direction. A control vector formed from p brackets can be produced using p controls with cosines at a single frequency ω and one cosine at a frequency of $p\omega$. To summarize, for vector fields generated from Lie brackets of control vector fields, motion can be generated with the following relations:

$$\begin{aligned} g_i \;&\rightarrow\; \alpha_i(t) \\ ad_{g_{i_1}} g_{i_2} \;&\rightarrow\; u_{i_1} = \alpha_{i_1}(t)\sin(\omega t) \\ &\qquad\; u_{i_2} = \alpha_{i_2}(t)\cos(\omega t) \\ ad_{g_{i_1}} ad_{g_{i_2}} g_{i_3} \;&\rightarrow\; u_{i_1} = \alpha_{i_1}(t)\cos(\omega t) \\ &\qquad\; u_{i_2} = \alpha_{i_2}(t)\cos(\omega t) \\ &\qquad\; u_{i_3} = \alpha_{i_3}(t)\cos(2\omega t) \\ &\qquad\; \vdots \end{aligned}$$

As shown in [10] for systems with drift, relations which will generate motion along the appropriate directions come by replacing each vector field in the above table with the appropriately corresponding term from the set of vector fields $\tilde{\mathcal{G}}$ constructed from Prop. 2.

Using these results and some knowledge of the Lie bracket structure of a nonlinear system, we can generate motion along desired directions and ultimately track given trajectories.

5 System Analysis and Experimental Results

For our model, the drift vector is zero when $[\dot{\psi}_1, \dot{\psi}_2, \dot{x}, \dot{y}, \dot{\theta}] = [0, 0, 0, 0, 0]$. However, at any point with zero velocity, all of the Lie brackets become zero. Thus, our system is not STLC. But if we consider the problem of trajectory tracking rather than stabilization or moving between two points, then we need only be concerned with satisfying the conditions for accessibility. I.e., we simply need to show that from a given point with nonzero velocity, we can move to another point with nonzero velocity.

Assuming nonzero velocity, we have the following correspondence for the joint positions and velocities:

$$\begin{aligned} \dot{\psi}_1 &\rightarrow g_1, \qquad \psi_1 \rightarrow ad_f g_1 \\ \dot{\psi}_2 &\rightarrow g_2, \qquad \psi_2 \rightarrow ad_f g_2 \end{aligned}$$

From (1), we can see that the elements of the vectors g_1 and g_2 are either zero or one. Thus the term $ad_{g_1} g_2$ is identically zero, and our system possesses the characteristics of (4). Due to the functional form of any higher level brackets, we are not able to determine linear independence of terms by symbolic calculation. We can, however, evaluate vector fields at particular points in the state space and argue by continuity that

characteristics of the vector fields at those points must hold in a neighborhood of the points. In particular, if the robot is moving straight ahead from the origin with no sideways or rotational velocity, we have the following correspondence:

$$\begin{aligned} \dot{x} &\rightarrow ad_{ad_f g_1} ad_f g_2 \\ \dot{\theta} &\rightarrow ad_{ad_f g_1} ad_{ad_f g_1} ad_f g_2 \\ x &\rightarrow ad_f ad_{ad_f g_1} ad_f g_2 \\ \theta &\rightarrow ad_f ad_{ad_f g_1} ad_{ad_f g_1} ad_f g_2 \end{aligned}$$

where the pairing is determined by the largest nonzero entry in the displayed vector field. Generally more than one entry will be nonzero, but in these cases, the given value dominates. Unfortunately, higher order brackets that have been tested have not produced independent motion in the y direction as well. One can argue that this coupling of y with the x and θ directions occurs because one cannot simply move the robot sideways but would need to achieve a parallel parking behavior. We are currently more interested with forward and turning gaits, so we will leave this issue to be addressed in the future and will restrict our attention to forward and rotational motions.

Given the state-bracket relations above and the results from the preceding section, we expect that we can achieve forward propulsion with system controls of the form

$$u_1 = \alpha_1 \sin(\omega t), \quad u_2 = -\alpha_2 \cos(\omega t)$$

and rotation with controls of the form

$$u_1 = \alpha_1 \cos(\omega t), \quad u_2 = \alpha_2 \cos(2\omega t).$$

The simulated response of our system model to each of these sets of controls with $\alpha_1 = \alpha_2 = 0.4$ in both cases, $\omega = 8$ for forward propulsion and $\omega = 3.5$ for turning gives the results shown respectively in Figs. 4 and 5. By simulation, we mean a numerical integration of the equations of motion. In each simulation, system parameters such as inertia and mass are taken from measurements on the experimental robot. In Fig. 4, the simulation shows that when the controls are turned on with the fish starting from rest, the body turns slightly. As the body velocity increases to a constant value, the fish orientation oscillates about this perturbed value, and the fish travels in a straight line. The turning gait, shown in Fig. 5, is primarily produced from the effects of added mass on the tail. This simulation predicts that when the fish is started from rest with this gait, the response of the body to the forces on the tail will be to initially pull backwards and to the side (due to scooping motions of the tail) before

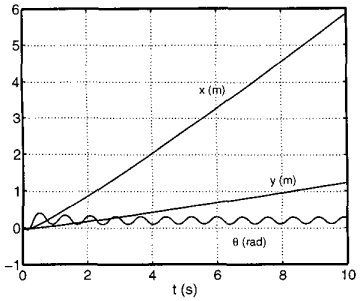

Figure 4: Simulated model response for forward propulsion.

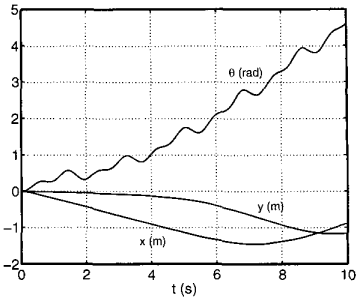

Figure 5: Simulated model response for turning.

settling into a circular motion. In both of these cases, we would like to draw attention to the fact that our model is based on quasi-static approximations of lift and drag, and we expect discrepancies between simulation and experiment during periods of large body acceleration such as when we start the body from zero velocity.

Considering the number of assumptions and simplifications made in this model, we do not expect that our robot will exactly produce these motions. Indeed, comparison of the above simulations and the following experiments demonstrates scaling discrepancies up to an order of magnitude. One likely source for these errors is the bearings in the trolley which are assumed to produce no stiction. Regardless, we do expect that the underlying nonlinear structure of the simulation and experiment will be the same. If this assumption is correct, then our robot should demonstrate the following behavior. First, for a forward propulsive gait, the robot should move forward without significant turning. Second, for a turning gait, the robot should turn significantly without large translational motions. Third, because g_1 and g_2 each appear once in the Lie bracket assumed to produce forward motion, the forward motion should scale linearly with the amplitude of u_1 and linearly with the amplitude of u_2. Fourth, because g_1 appears twice in the Lie bracket associated with turn-

ing and g_2 appears once, turning should scale linearly with the amplitude of u_2 and quadratically with the amplitude of u_1.

In Figs. 6-8 we show recorded experimental results for application of controls of the form $u_1(t) = \alpha_1 \sin(8t)$, $u_2(t) = -\alpha_2 \cos(8t)$ with $\alpha_i = \{0.1, 0.2, 0.3, 0.4\}$. The typical response shown in Fig. 6 demonstrates the same behavior as the simulation where the body moves in a straight line and oscillates slightly about that direction. The average orientation is not a fixed value due to system disturbances from motion of the water and tension in the vehicle power and communication cables. Our prediction was that

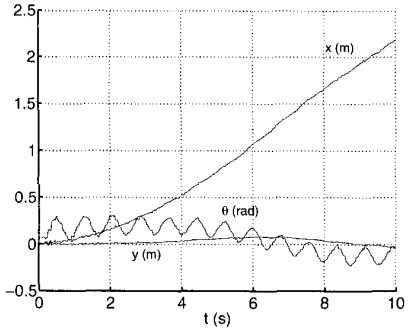

Figure 6: Experimental data for forward propulsion with $\alpha_1 = \alpha_2 = 0.4$.

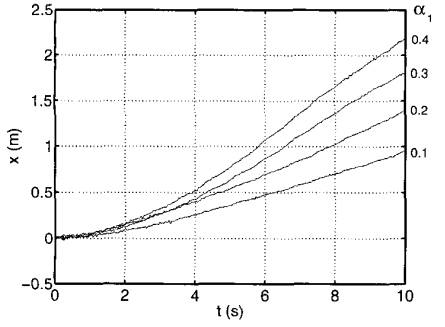

Figure 7: Experimental data for forward propulsion with $\alpha_1 = \{0.1, 0.2, 0.3, 0.4\}$ and $\alpha_2 = 0.4$.

forward motion in this direction corresponds to a single bracket and that the net motion should scale linearly and symmetrically with the amplitudes of each of the controls. Clearly, our experimental results do validate this hypothesis.

We now consider turning maneuvers. Interestingly, our analysis predicts turning maneuvers for inputs of the form $u_1(t) = \alpha_1 \cos(3.5t)$, $u_2(t) = \alpha_2 \cos(7t)$. Figs. 9-11 show experimental results for application of these

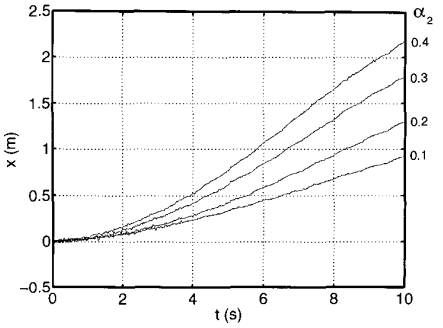

Figure 8: Experimental data for forward propulsion with $\alpha_1 = 0.4$ and $\alpha_2 = \{0.1, 0.2, 0.3, 0.4\}$.

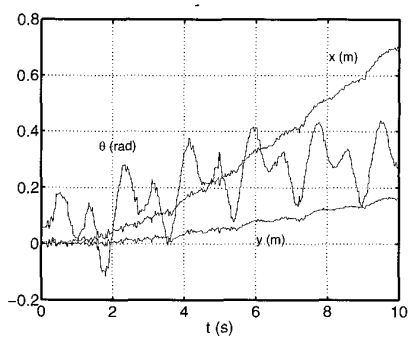

Figure 9: Experimental data for turning motion with $\alpha_1 = \alpha_2 = 0.4$.

controls with $\alpha_i = \{0.1, 0.2, 0.3, 0.4\}$. This data illustrates two things. First, the fish actually turns as predicted by the theory. Unlike the simulation, however, the body is not pulled backward by the initial tail kick. Stiction in the bearings and inaccurate model drag coefficients could account for this behavior. Second, for a turning motion, our model predicts that a second level bracket where g_1 appears twice and g_2 appears once should produce the desired behavior. As discussed above, because g_1 appears twice, we expect net motion to scale quadratically with α_1. Because g_2 appears once we expect net motion to to scale linearly in the amplitude of u_2. The amplitudes that we are using for our inputs are all less than one, so doubling α_1 with α_2 unchanged should produce less net increase in θ than doubling α_2 with α_1 unchanged. The data in the figures does indeed support this expectation with the net turn much more strongly affected by changes in α_2 than in α_1.

6 Conclusions and Future Work

We have developed a control affine model to which we are able to apply nonlinear control methods to pro-

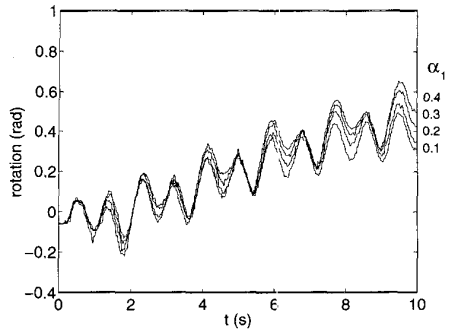

Figure 10: Experimental data for turning motion with $\alpha_1 = \{0.1, 0.2, 0.3, 0.4\}$ and $\alpha_2 = 0.4$.

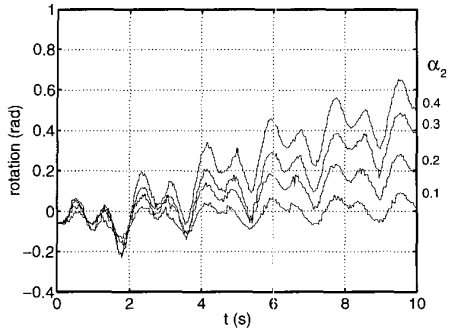

Figure 11: Experimental data for turning motion with $\alpha_1 = 0.4$ and $\alpha_2 = \{0.1, 0.2, 0.3, 0.4\}$.

duce forward propulsion and turning gaits. The qualitative trends of our experiments do correspond well to the theoretically predicted behavior. A key aspect of this work is the fact that we are able to produce these results with an extremely simplified model that captures only the most basic of system effects. Also, we must emphasize that these methods are open-loop: no state feedback is used to produce the motions.

Several avenues of investigation are now available for exploration. Due to the complicated nature of the equations of motion, we have had to resort to numerical methods for part of our analysis. This situation is not unique to our system, and appropriate numerical tools for evaluating system controllability characteristics must be developed. Given that we can generate motions in two independent state directions, we wish to track trajectories in those directions. Open-loop methods exist for this task if the system model is known exactly and if system initial conditions can be dictated exactly. In general neither situation exists. Our current research effort is directed toward the construction of feedback control functions which enable tracking in the presence of inexact system models.

References

[1] J. M. Anderson and P. A. Kerrebrack. The vorticity control unmanned undersea vehicle–an autonomous vehicle employing fish swimming propulsion and maneuvering. In *Proc. 10th Int. Symp. on unmanned untethered submersible technology*, pages 189–195, Durham, NH, September 1997.

[2] D. Barrett, M. Grosenbaugh, and M. S. Triantafyllou. The optimal control of a flexible hull robotic undersea vehicle propelled by an oscillating foil. In *Proc. 1996 Symp. Aut. Underwater Vehicle Tech.*, pages 1–9, 1996.

[3] S. Childress. *Mechanics of Swimming and Flying.* Cambridge University Press, Cambridge, 1981.

[4] S. D. Kelly, R. J. Mason, C. T. Anhalt, R. M. Murray, and J. W. Burdick. Modelling and experimental investigation of carangiform locomotion for control. In *Proc. of the 1998 Amer. Cont. Conf.*, pages 1271–1276, 1998.

[5] P. Y. Li and S. Saimek. Modeling and estimation of hydrodynamic potentials. In *Proceedings of the 1999 CDC*, pages 3253–3258, 1999.

[6] J. L. Lighthill. *Mathematical Biofluiddynamics.* SIAM, Philadelphia, 1975.

[7] W. Liu. An approximation algorithm for nonholonomic systems. *SIAM J. Control. Opt.*, 35(4):1328–1365, July 1997.

[8] R. J. Mason and J. W. Burdick. Construction and modelling of a carangiform robotic fish. In *1999 International Symposium on Experimental Robotics,* 1999.

[9] R. J. Mason and J. W. Burdick. Experiments in carangiform robotic fish locomotion. In *Proceedings of the 2000 ICRA*, pages 428–435, 2000.

[10] K. A. Morgansen. *Temporal patterns in learning and control.* PhD thesis, Harvard University, 1999.

[11] K. A. Morgansen and R. W. Brockett. Nonholonomic control based on approximate inversion. In *Proc. of the 1999 American Control Conference*, pages 3515–3519, 1999.

[12] R. M. Murray and S. Sastry. Nonholonomic motion planning: Steering using sinusoids. *IEEE Trans. Aut. Cont.*, 38(5):700–716, 1993.

[13] J. N. Newman and T. Y. Wu. Hydrodynamical aspects of fish swimming. In T. Wu, C. Brokaw, and C. Brennen, editors, *Swimming and Flying in Nature, Vol 2.*, pages 615–634. Plenum Press, New York, 1975.

[14] H. J. Sussmann and J. Jurdjevic. Controllability of nonlinear systems. *J. Diff. Eqns.*, 12:95–116, 1972.

[15] M. S. Triantafyllou and G. S. Triantafyllou. An efficient swimming machine. *Scientific American*, pages 64–70, March 1995.

[16] M. J. Wolfgang, J. M. Anderson, M. A. Grosenbaugh, D. K. P Yue, and M. S. Triantafyllou. Near-body flow dynamics in swimming fish. *J. Experimental Biology*, 202(17):2303–2307, 1999.